Quantum Signature of a Squeezed Mechanical Oscillator

A. Chowdhury,[1] P. Vezio,[2] M. Bonaldi,[3,4] A. Borrielli,[3,4] F. Marino,[5,1] B. Morana,[3,6] G. A. Prodi,[4,7] P. M. Sarro,[6] E. Serra,[4,6] and F. Marin[1,2,5,8,*]

[1]*CNR-INO, L.go Enrico Fermi 6, I-50125 Firenze, Italy*
[2]*European Laboratory for Non-Linear Spectroscopy (LENS), Via Carrara 1, I-50019 Sesto Fiorentino (FI), Italy*
[3]*Institute of Materials for Electronics and Magnetism, Nanoscience-Trento-FBK Division, 38123 Povo, Trento, Italy*
[4]*Istituto Nazionale di Fisica Nucleare (INFN), Trento Institute for Fundamental Physics and Application, I-38123 Povo, Trento, Italy*
[5]*INFN, Sezione di Firenze, Via Sansone 1, I-50019 Sesto Fiorentino (FI), Italy*
[6]*Dept. of Microelectronics and Computer Engineering /ECTM/DIMES, Delft University of Technology, Feldmanweg 17, 2628 CT Delft, Netherlands*
[7]*Dipartimento di Fisica, Università di Trento, I-38123 Povo, Trento, Italy*
[8]*Dipartimento di Fisica e Astronomia, Università di Firenze, Via Sansone 1, I-50019 Sesto Fiorentino (FI), Italy*

(Received 17 July 2019; published 13 January 2020)

Recent optomechanical experiments have observed nonclassical properties in macroscopic mechanical oscillators. A key indicator of such properties is the asymmetry in the strength of the motional sidebands produced in the probe electromagnetic field, which is originated by the noncommutativity between the oscillator ladder operators. Here we extend the analysis to a squeezed state of an oscillator embedded in an optical cavity, produced by the parametric effect originated by a suitable combination of optical fields. The motional sidebands assume a peculiar shape, related to the modified system dynamics, with asymmetric features revealing and quantifying the quantum component of the squeezed oscillator motion.

DOI: 10.1103/PhysRevLett.124.023601

The quantum description of the microscopic world is verified with ever increasing accuracy, and more and more common and indispensable technologies are based on intrinsically quantum principles. On the other hand, some features predicted by quantum mechanics are in contrast with the everyday experience, in particular those originated by entanglement and by the Heisenberg uncertainty principle, encoded in the noncommutativity of some measurable operators. It is therefore not only interesting from the scientific and technological point of view, but also useful for extending our intuitive grasp of quantum devices, to verify how such behaviors are conserved and/or modified in the transition between microscopic and macroscopic reality.

A relevant contribution in this direction is being given by optomechanical experiments [1] that allowed us, in the last decade, to realize systems of macroscopic mechanical oscillators exhibiting nonclassical properties. A key example is the asymmetry in the motional sidebands generated in an electromagnetic probe field [2–7]. As far as spurious experimental features are avoided [8–10], this asymmetry becomes a footprint of the quantum motion of the oscillator, being originated by the noncommutativity between its ladder operators [11–13]. The sideband asymmetry is measurable whenever the thermal agitation is weak enough, and therefore for low phonon numbers.

A further step on the path highlighting quantum features in macroscopic systems is the realization of strongly nonclassical states. In this work we turn our attention to the squeezed state of a macroscopic mechanical oscillator embedded in an optical cavity and identify a clear signature of its quantum nature.

The coordinate expressing the position of a harmonic oscillator can be written as $x = 2x_{\mathrm{zpf}}[X\cos(\Omega_m t + \phi) + Y\sin(\Omega_m t + \phi)]$, where x_{zpf} is the ground state spread of the position (i.e., $x_{\mathrm{zpf}} = \sqrt{\hbar/2m\Omega_m}$ where m is the mass and Ω_m the frequency of the oscillator). The quadratures X and Y are slowly varying if the oscillator is damped. In a thermal state, the variance of the quadratures is $\langle X^2\rangle = \langle Y^2\rangle = (2\bar{n}_{\mathrm{th}} + 1)/4$, where $\bar{n}_{\mathrm{th}}$ is the mean thermal occupation number, for any choice of the phase ϕ. The mechanical interaction of the oscillator with a readout electromagnetic field produces in the latter motional sidebands around its main field frequency, displaced by $\pm\Omega_m$, and proportional, respectively, to $\hat{b} = X + iY$ (anti-Stokes sideband) and $\hat{b}^\dagger = X - iY$ (Stokes sideband). In a thermal state, the variances of $\hat{b}$ and $\hat{b}^\dagger$ are, respectively, $\langle\hat{b}^\dagger\hat{b}\rangle = \bar{n}_{\mathrm{th}}$ and $\langle\hat{b}\hat{b}^\dagger\rangle = \bar{n}_{\mathrm{th}} + 1$ [14]. In cavity optomechanics experiments, the electromagnetic field competes with the thermal environment yielding, in appropriate conditions, a larger overall coupling rate Γ_{eff}, a mechanical resonance frequency modified by the optical spring effect, and a lower mean phonon number $\bar{n}$ [1,15]. The ratio between Stokes and anti-Stokes sidebands can now be written as $R = (\bar{n} + 1)/\bar{n}$ and, for low enough $\bar{n}$, a deviation from unity of R becomes measurable, providing a clear signature of the

smooth transition between the classical motion and the quantum behavior. In the case of continuous measurements on a weakly coupled oscillator (with $\Gamma_{\rm eff} \ll \Omega_m$), the observed variables (either x, or the quadratures, or the sidebands) exhibit Lorentzian spectra with width $\Gamma_{\rm eff}$, and their variance can be evaluated by integrating over the respective spectral peaks.

In the absence of an intrinsic reference phase, all the quadratures (for any choice of ϕ) are obviously indistinguishable. On the other hand, a phase-sensitive interaction can break such symmetry and provide, e.g., different variances in two orthogonal quadratures. In this case the oscillator is said to be in a squeezed state. A scheme that allowed us to obtain it in cavity opto-mechanical experiments is the so-called reservoir engineering [16,17]. In this configuration, unbalanced fields are detuned, respectively, by $\pm\Omega_m$ from the cavity resonance. Because of the interference between the noise sidebands of the two fields, the electromagnetic reservoir seen by the mechanical oscillator is modified in a phase-sensitive way. When its effect dominates over the thermal one, the result is a squeezed oscillator. It has been observed in microwave experiments with cooled nano oscillators [18–21], where the variance in one quadrature was indeed reduced below that of the ground state (i.e., $\langle X^2\rangle < 1/4$ for a particular value of ϕ). This noise reduction can play an important role, e.g., in optimizing the sensitivity of the oscillator used as a quantum sensor. However, we point out that the motional sidebands remain unmodified and a more direct evidence of nonclassical behavior is lacking.

A different possibility to produce a squeezed state of the oscillator is the modulation of its spring constant at twice its resonance frequency (parametric modulation) [22]. This scheme has been implemented in several experiments with thermal oscillators, including cavity optomechanical setups where a modulation of the optical spring is obtained by acting on the light intensity or frequency [23,24]. The variances in two, suitably chosen, orthogonal quadratures are altered, respectively, by factors of $1/(1+s)$ and $1/(1-s)$, where s is the parametric gain. The correspondent spectra keep Lorentzian shapes with modified widths, given, respectively, by $\Gamma_+ = \Gamma_{\rm eff}(1+s)$ (overdamped quadrature) and $\Gamma_- = \Gamma_{\rm eff}(1-s)$ (underdamped quadrature). It is thus interesting to consider what happens to the spectra of the motional sidebands that are somehow given by linear combinations of the two quadratures. The spectrum of each sideband turns out to be composed of two Lorentzian curves, with width Γ_+ and Γ_-. More relevant, the areas of this two Lorentzian components are different in the two sidebands, with ratios given by

$$R_+ = \frac{\bar{n}+1+s/2}{\bar{n}-s/2}, \tag{1}$$

$$R_- = \frac{\bar{n}+1-s/2}{\bar{n}+s/2}, \tag{2}$$

respectively, for the broader (R_+) and narrower (R_-) components. If the oscillator motion is described by classical (commuting) variables, the two sidebands' spectra must be identical, and the same happens in a quantum description of a "classical" (i.e., thermal noise dominated, with $\bar{n} \gg 1$) oscillator. On the other hand, for moderately low $\bar{n}$ the sideband ratios R_+ and R_- differ not only from unity, but also from the ratio R measurable without parametric squeezing. Namely, the ratio is stronger for the broadened Lorentzian component, while it approaches the unity for the narrowed component as $s \to 1$ (i.e., close to the parametric instability threshold). Therefore, a purely quantum effect can be put into evidence even for a state having a variance exceeding that of the ground state in any quadrature and, besides thermal noise, even for states that are not of minimal uncertainty (i.e., with $\langle X^2\rangle\langle Y^2\rangle > 1/16$) as those created by parametric squeezing.

In the following, we describe an experimental study of this effect, and we show that a nonclassical state of the macroscopic mechanical oscillator is realized through interaction with optical fields.

The experimental setup is sketched in Fig. 1. The measurements are performed on a circular SiN membrane with a thickness of 100 nm and a diameter of 1.64 mm, supported by a silicon "loss shield" structure [25–28]. In this work we exploit the (0,2) mechanical mode at ~530 kHz, having a quality factor of 6.4×10^6 at cryogenic temperature (mechanical linewidth 0.08 Hz).

The oscillator is placed in a Fabry-Perot cavity of length 4.38 mm, at 2 mm from the cavity flat end mirror, forming a "membrane-in-the-middle" setup [29], where the single-photon coupling rate with the (0,2) mechanical mode is $g_0/2\pi \simeq 30$ Hz. The input coupler is concave with a radius

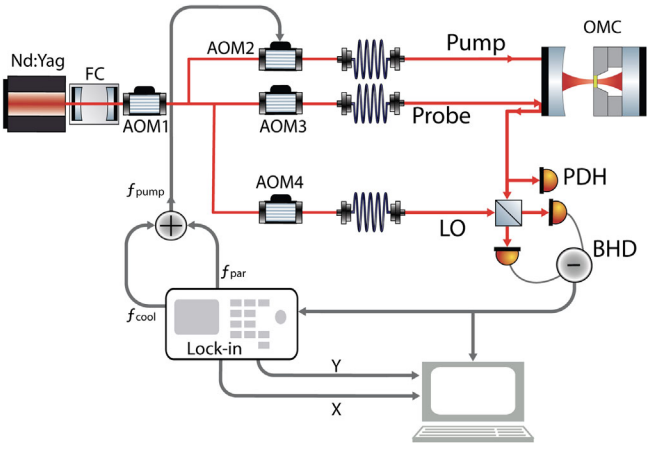

FIG. 1. Sketch of the experimental setup (see text) and conceptual scheme of the field frequencies. The LO is placed on the blue side of the probe (ω_p) and detuned by $\Delta_{LO} \ll \Omega_m$, therefore the Stokes lines are on the red side of the LO, while the anti-Stokes lines are on the blue side. In the heterodyne spectra, they are located, respectively, at $\Omega_m + \Delta_{LO}$ (Stokes) and $\Omega_m - \Delta_{LO}$ (anti-Stokes).

of 50 mm, originating a waist of 70 μm. The cavity finesse and linewidth are, respectively, 20 000 and $\kappa = 1.7\ \mathrm{MHz} \times 2\pi$. The optomechanical cavity is cooled down to $\sim$7 K in a helium flux cryostat, yielding a thermal occupation number of 2.6×10^5 for the considered mechanical mode. More details on the optomechanical system and its characterization are reported and discussed in Ref. [30].

The light of a Nd:YAG laser is filtered by a Fabry-Perot cavity (linewidth of 66 kHz) and split into three beams, whose frequencies are controlled by means of acousto-optic modulators (AOM) and sent to the experimental bench by optical fibers [Fig. 1(a)]. The probe beam, at frequency ω_p, is kept resonant with the optomechanical cavity (OMC) using the Pound-Drever-Hall (PDH) detection, with a servo loop exploiting AOM1 to follow fast fluctuations and a piezoelectric transducer to compensate for long-term drifts of the cavity length. About 2 μW of the reflected probe are sent to the PDH detection, while most of the probe light ($\sim$10 μW) is combined with the local oscillator (LO) beam ($\sim$2 mW) in a balanced detection (BHD). The LO frequency ω_{LO} is shifted with respect to the probe (namely, by $\Delta_{\mathrm{LO}}/2\pi = 11$ kHz), to realize a low-frequency heterodyne detection [31]. The output of the BHD is acquired and also sent to a lock-in amplifier and demodulated at $\Omega_{\mathrm{par}}/2$ (where Ω_{par} is defined later). The two quadrature outputs of the lock-in are simultaneously acquired and off-line processed.

The third beam (pump beam), orthogonally polarized with respect to the probe, is also sent to the cavity. Its field contains a main, cooling tone at a frequency ω_{cool} red detuned from the cavity resonance, and a modulation tone at a frequency ω_{par}, blueshifted with respect to ω_{cool}. The two tones are obtained by driving the AOM2 with the sum of two radiofrequency signals. To realize the parametric drive of the oscillator, the frequency difference between the two tones is $\Omega_{\mathrm{par}} = (\omega_{\mathrm{par}} - \omega_{\mathrm{cool}}) \equiv 2\Omega_m$. To obtain comparable oscillator spectra in the absence of coherent parametric drive, we further shift the modulation tone by $\sim$12 kHz, i.e., by a quantity larger than the mechanical width (that is typically $\Gamma_{\mathrm{eff}}/2\pi \simeq 4$ kHz), but much smaller than the cavity width. The optomechanical effect of the modulation tone is thus maintained almost constant, but the coherent effect of the two tones on the oscillator is avoided. During the measurements, the two values of the modulation tone frequency are alternated every 5 s and the corresponding periods extracted from the acquired time series are analyzed separately. In this way, we can compare the two situations (with and without coherent parametric drive) keeping the same system conditions, avoiding the effect of possible long term drifts.

All the radiofrequency sinusoidal signals used in the experiment, for driving the AOMs and as reference in the lock-in amplifier, are kept phase coherent. The system thus realizes a phase-sensitive heterodyne detection.

Typical heterodyne spectra are shown in Figs. 2(a), 2(c), together with the corresponding spectra of two orthogonal quadratures [Figs. 2(b), 2(d)]. For the latter, the demodulation phase is chosen in order to produce maximally squeezed quadratures in the case of resonant parametric drive.

The spectra shown in the upper panels [Figs. 2(a), 2(b)] are obtained without coherent parametric effect. The heterodyne spectrum consists of the two motional sidebands, separated by $2\Delta_{\mathrm{LO}}$, whose signal shapes are fitted by Lorentzian curves having the same width Γ_{eff}. The ratio R of their areas, corrected for the residual probe detuning as described in Ref. [30], allows us to extract the oscillator occupation number $\bar{n}$ according to $R = 1 + 1/\bar{n}$. As shown with green symbols in Fig. 3, R remains almost constant when varying the relative strength of the pump tones. A theoretical curve, based on independently measured parameters, shows indeed a weak dependence due to the different cooling efficiency of the two pump tones. The agreement of this curve with the experimental data is good, and an extensive characterization of our system [30] further confirms the reliability of the measurement of $\bar{n}$.

In the spectra of each quadrature [Figs. 2(b), 2(d)], the mechanical peak is visible at frequencies around $\Omega = \Delta_{\mathrm{LO}}$, and is originated by the superposition of the two motional sidebands. Each spectrum is fitted by the sum of two equal Lorentzian shapes centered at $\pm\Delta_{\mathrm{LO}}$:

$$S(\Omega) = \sigma_0^2 \left(\frac{\Gamma/2}{(\Omega - \Delta_{\mathrm{LO}})^2 + (\Gamma/2)^2} + \frac{\Gamma/2}{(\Omega + \Delta_{\mathrm{LO}})^2 + (\Gamma/2)^2} \right). \tag{3}$$

Without parametric effect Fig. 2(b), the Lorentzian curves fitting the two quadratures turn out to be equal within the statistical uncertainty, and their width matches Γ_{eff} extracted from the corresponding heterodyne spectra. On the other hand, in the case of resonant parametric drive, the spectra of the two quadratures [Fig. 2(d)] become, respectively, broader and narrower with respect to the previous case. The fitting function remains the same (3), but with different areas ($\sigma^2_{X,Y}$) and widths ($\Gamma_{X,Y}$) for the two quadratures. The variances of the two quadratures, normalized to σ_0^2, are shown in Fig. 4 as a function of the ratio between modulation and cooling tones, keeping a constant total pump power. Dashed lines show the expected behaviors, i.e., respectively, $1/(1+s)$ and $1/(1-s)$, where the parametric gain s is calculated using the measured pump tones ratio and detuning, and the cavity width κ. It can be expressed as $s = \Gamma_{\mathrm{par}}/\Gamma_{\mathrm{eff}}$, with [32]

$$\Gamma_{\mathrm{par}} = \frac{4g^2 \sqrt{\epsilon_c(1-\epsilon_c)}\,\Delta_{\mathrm{pump}}}{\Delta^2_{\mathrm{pump}} + \kappa^2/4} \tag{4}$$

and

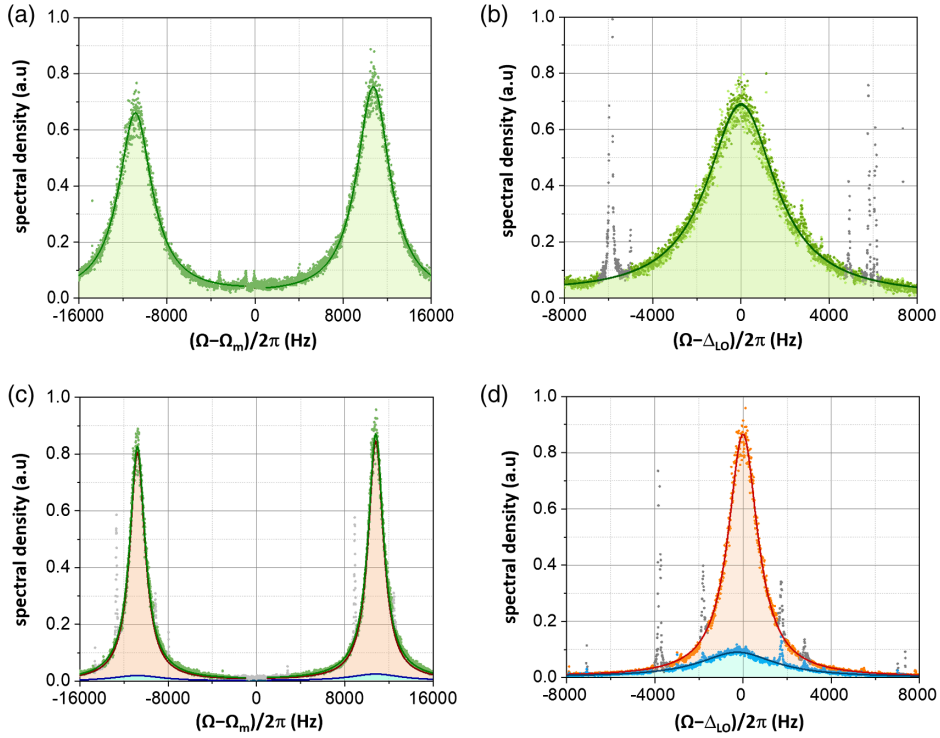

FIG. 2. (a),(c) Heterodyne spectra (without demodulation) around the (0,2) membrane mode at $\Omega_m/2\pi \simeq 530$ kHz, (a) without parametric drive and (c) with parametric drive. In (a) the spectrum is fitted by Lorentzian curves (solid line). In (c) the fitting function (dark green line) is the superposition of a broad and a narrow Lorentzian shape, whose contributions are shown with blue and red lines. (b),(d) Spectra of the fluctuations in two quadratures, obtained by phase-sensitive demodulation of the heterodyne signal at $\Omega_{\mathrm{par}}/2$, (b) without parametric drive and (d) with parametric drive. In (b) the two spectra (dark and light green symbols) are not distinguishable, and one single Lorentzian fit is shown (solid line). In (d) the two spectra (orange and blue symbols) are fitted with different Lorentzian curves (red and blue solid lines). The full vertical scales correspond, respectively, to 2 $\mathrm{Hz}^2/\mathrm{Hz}$ (a),(b), 4 $\mathrm{Hz}^2/\mathrm{Hz}$ (c), 8 $\mathrm{Hz}^2/\mathrm{Hz}$ (d).

$$\Gamma_{\mathrm{eff}} = \Gamma_m + g^2\kappa\left(\frac{\epsilon_c}{\Delta_{\mathrm{pump}}^2+\kappa^2/4} - \frac{\epsilon_c}{(\Delta_{\mathrm{pump}}-2\Omega_m)^2+\kappa^2/4} + \frac{1-\epsilon_c}{(\Delta_{\mathrm{pump}}+2\Omega_m)^2+\kappa^2/4} - \frac{1-\epsilon_c}{\Delta_{\mathrm{pump}}^2+\kappa^2/4}\right)$$

(g is the total optomechanical coupling strength of the pump beam, ϵ_c is the ratio between cooling tone power and total pump power, Δ_{pump} is the mean detuning of the pump tones with respect to the cavity resonance, and Γ_m is the mechanical width in the absence of optomechanical effects). We stress that in the expression of s, the optomechanical coupling g disappears, eliminating the necessity of its, not obvious, evaluation. The shown theoretical lines are calculated with no free parameters, and we remark on their excellent agreement with the experimental data.

The described imbalance between the fluctuations of the two quadratures is the characteristics of a squeezed state, but distinguishing a classical (thermal) state from a quantum state on this basis is not straightforward. The qualitative behavior is the same, therefore an accurate absolute calibration of the displacement variance and its comparison with that of the ground state are necessary. In the absence of parametric drive, the measured occupation number is here $\bar{n} = 5.8$, therefore the variance in each quadrature is still $\sim$12 times larger than in the ground state. At the maximum displayed squeezing, σ_Y^2 is reduced by a factor of 0.66, remaining well above that of the ground state. However, as we will show, the heterodyne spectrum already provides a direct quantum signature of the squeezed state. This is the most important result of our work. The spectral shape of each motional sideband departs from a simple Lorentzian peak, and it is indeed fitted by the sum of two Lorentzian curves with the same center, but different amplitudes and widths Fig. 2(c). For the fitting procedure on the pair of motional sidebands we have used four independent Lorentzian amplitudes, and two widths written as $\Gamma_+ = \Gamma_{\mathrm{eff}}(1+s)$ and $\Gamma_- = \Gamma_{\mathrm{eff}}(1-s)$, where Γ_{eff} is fixed to the value derived from the corresponding spectra in the absence of resonant parametric drive. Γ_+ and Γ_- agree, within the statistical uncertainty, respectively, with Γ_Y and Γ_X. Moreover, the parametric gain s obtained from the fitted Lorentzian widths is in agreement with its estimate extracted from the variances of the two quadratures. This is displayed in Fig. 4, where we show with circles the values of $(1+s)$ and $(1-s)$ given by the widths of the heterodyne spectra. We remark here the overall coherence between measurements of the variance in the quadratures (squares), measurements of the widths of the Lorentzian

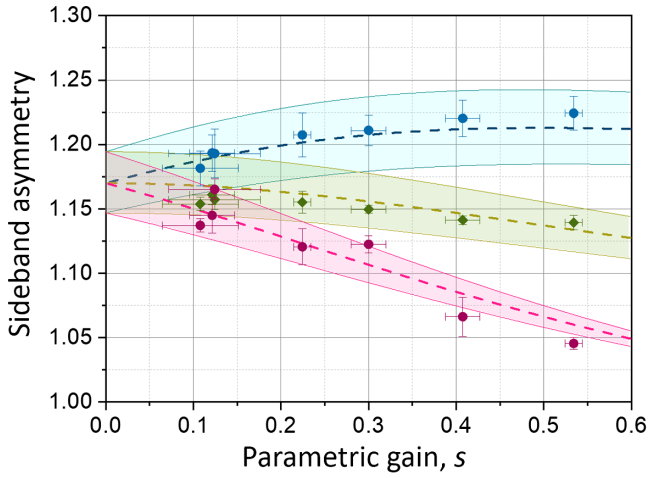

FIG. 3. Green symbols: sideband asymmetry R with no parametric drive (i.e., with detuned modulation tone), for increasing power in the modulation tone. Sideband ratios R_+ (blue circles) and R_- (red circles) with coherent parametric drive. The values of s in the abscissa are extracted from the fitted widths $\Gamma_+ = \Gamma_{\rm eff}(1+s)$ and $\Gamma_- = \Gamma_{\rm eff}(1-s)$. Dashed lines show the corresponding theoretical behavior, with shadowed areas given by the uncertainty in the system parameters (in particular, 5% in the cavity width and 0.5 K in the temperature). Error bars reflect the standard deviations in 5 consecutive independent measurements, each one lasting 100 s. The total pump power is kept constant during all the measurements.

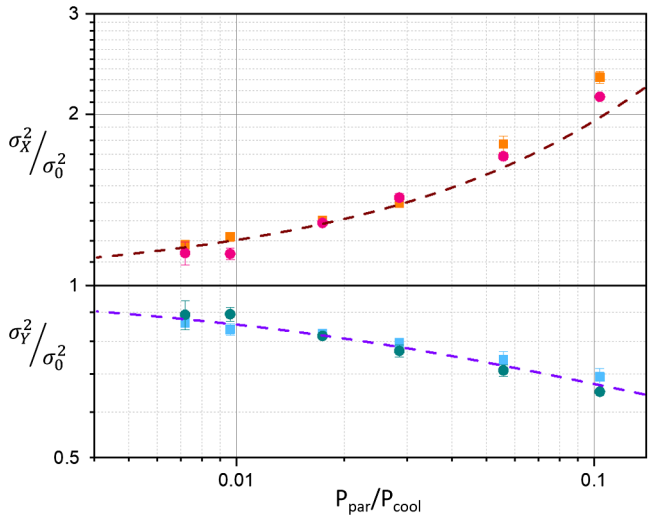

FIG. 4. Variance in the X (orange squares) and Y (cyan squares) quadratures, normalized to σ_0^2, as a function of the ratio between modulation and cooling tones, for constant total pump power. Dashed lines show the theoretical behavior. Magenta and blue circles are the correspondent expected values, calculated, respectively, as $1/(1-s)$ and $1/(1+s)$, where s is extracted from the width of the broad and narrow Lorentzian contributions in the heterodyne spectra. Error bars reflect the standard deviations in 5 consecutive independent measurements, each one lasting 100 s.

components in the heterodyne spectra (circles), and the theoretical model (dashed lines).

The four areas of the Lorentzian components allow us to calculate one sideband's asymmetry R_- for the narrower Lorentzian peak, and one R_+ for the broader peak. These ratios are plotted in Fig. 3 as a function of the parametric gain s. The theoretical spectra of the Stokes and anti-Stokes sidebands are proportional, respectively, to [32]

$$S_{\hat{b}^\dagger\hat{b}^\dagger} = \frac{\Gamma_{\rm eff}}{2}\left[\frac{1+\bar{n}-s/2}{\Omega^2+\Gamma_-^2/4}+\frac{1+\bar{n}+s/2}{\Omega^2+\Gamma_+^2/4}\right], \tag{5}$$

$$S_{\hat{b}\hat{b}} = \frac{\Gamma_{\rm eff}}{2}\left[\frac{\bar{n}+s/2}{\Omega^2+\Gamma_-^2/4}+\frac{\bar{n}-s/2}{\Omega^2+\Gamma_+^2/4}\right]. \tag{6}$$

The ratios between the areas of the broad and narrow Lorentzian components give the expressions (1), (2). The latter theoretical curves are also traced in Fig. 3, without free-fitting parameters. The agreement with the experimental measurements is an indication that the overall understanding of the system is correct. Even with a moderately warm oscillator the analysis of the motional sidebands allows us to extract and explore the quantum component of the motion of the mechanical oscillator in a squeezed state.

These results show that, as it happens for the thermal states of the oscillator, even for the squeezed state the transition between classical and quantum behavior is smooth, and a nonclassical squeezing indicator is in principle measurable at any temperature. In other words, the quantum dynamics is present even in macroscopic oscillators dominated by thermal noise. It is, however, interesting to consider what should happen when the fluctuations in the squeezed quadrature are reduced below those of the ground state. This occurs for $(2\bar{n}+1)/(1+s) < 1$, i.e., for $s > 2\bar{n}$. From Eq. (6) we see that the broad Lorentzian contribution to the anti-Stokes sideband becomes negative (even if, of course, the overall spectral density remains positive for any Ω). This is a threshold providing a clear indication that one is entering the *bona fide* quantum squeezing regime, without the necessity of absolute calibrations (we stress however that the increased sideband asymmetry is already a *per se* quantum feature). The stationary parametric drive is stable for $s < 1$, therefore the above condition requires an initial occupation number $\bar{n} < 0.5$. For thermal oscillators, several techniques have been conceived and demonstrated to overcome the parametric instability threshold, based on weak measurements and feedback [23,24,33–36]. The extension of our analysis to this regime, as well as to the evolution of nonstationary squeezed states [37], would provide additional insight to the quantum behavior of macroscopic mechanical systems, particularly useful for developing new protocols in the field of quantum sensing.

Research performed within the Project QuaSeRT funded by the QuantERA ERA-NET Cofund in Quantum Technologies implemented within the European Union's Horizon 2020 Programme. The research has been partially supported by INFN (HUMOR project).

*marin@fi.infn.it

[1] M. Aspelmeyer, T. J. Kippenberg, and F. Marquardt, Rev. Mod. Phys. **86**, 1391 (2014).

[2] A. H. Safavi-Naeini, J. Chan, J. T. Hill, T. P. M. Alegre, A. Krause, and O. Painter, Phys. Rev. Lett. **108**, 033602 (2012).

[3] T. P. Purdy, P. L. Yu, N. S. Kampel, R. W. Peterson, K. Cicak, R. W. Simmonds, and C. A. Regal, Phys. Rev. A **92**, 031802(R) (2015).

[4] M. Underwood, D. Mason, D. Lee, H. Xu, L. Jiang, A. B. Shkarin, K. Børkje, S. M. Girvin, and J. G. E. Harris, Phys. Rev. A **92**, 061801(R) (2015).

[5] R. W. Peterson, T. P. Purdy, N. S. Kampel, R. W. Andrews, P. L. Yu, K. W. Lehnert, and C. A. Regal, Phys. Rev. Lett. **116**, 063601 (2016).

[6] V. Sudhir, D. J. Wilson, R. Schilling, H. Schutz, S. A. Fedorov, A. H. Ghadimi, A. Nunnenkamp, and T. J. Kippenberg, Phys. Rev. X **7**, 011001 (2017).

[7] L. Qiu, I. Shomroni, P. Seidler, and T. Kippenberg, arXiv:1903.10242.

[8] A. M. Jayich, J. C. Sankey, K. Børkje, D. Lee, C. Yang, M. Underwood, L. Childress, A. Petrenko, S. M. Girvin, and J. G. E. Harris, New J. Phys. **14**, 115018 (2012).

[9] A. H. Safavi-Naeini, J. Chan, J. T. Hill, S. Gröblacher, H. Miao, Y. Chen, M. Aspelmeyer, and O. Painter, New J. Phys. **15**, 035007 (2013).

[10] L. Qiu, I. Shomroni, M. A. Ioannou, N. Piro, D. Malz, A. Nunnenkamp, and T. J. Kippenberg, Phys. Rev. A **100**, 053852 (2019).

[11] F. Y. Khalili, H. Miao, H. Yang, A. H. Safavi-Naeini, O. Painter, and Y. Chen, Phys. Rev. A **86**, 033840 (2012).

[12] A. J. Weinstein, C. U. Lei, E. E. Wollman, J. Suh, A. Metelmann, A. A. Clerk, and K. C. Schwab, Phys. Rev. X **4**, 041003 (2014).

[13] K. Børkje, Phys. Rev. A **94**, 043816 (2016).

[14] A. A. Clerk, M. H. Devoret, S. M. Girvin, F. Marquardt, and R. J. Schoelkopf, Rev. Mod. Phys. **82**, 1155 (2010).

[15] O. Arcizet, P. F. Cohadon, T. Briant, M. Pinard, and A. Heidmann, Nature (London) **444**, 71 (2006).

[16] F. Verstraete, M. M. Wolf, and J. I. Cirac, Nat. Phys. **5**, 633 (2009).

[17] A. Kronwald, F. Marquardt, and A. A. Clerk, Phys. Rev. A **88**, 063833 (2013).

[18] E. E. Wollman, C. U. Lei, A. J. Weinstein, J. Suh, A. Kronwald, F. Marquardt, A. A. Clerk, and K. C. Schwab, Science **349**, 952 (2015).

[19] J. M. Pirkkalainen, E. Damskagg, M. Brandt, F. Massel, and M. A. Sillanpaa, Phys. Rev. Lett. **115**, 243601 (2015).

[20] F. Lecocq, J. B. Clark, R. W. Simmonds, J. Aumentado, and J. D. Teufel, Phys. Rev. X **5**, 041037 (2015).

[21] C. U. Lei, A. J. Weinstein, J. Suh, E. E. Wollman, A. Kronwald, F. Marquardt, A. A. Clerk, and K. C. Schwab, Phys. Rev. Lett. **117**, 100801 (2016).

[22] D. Rugar and P. Grütter, Phys. Rev. Lett. **67**, 699 (1991).

[23] A. Pontin, M. Bonaldi, A. Borrielli, F. S. Cataliotti, F. Marino, G. A. Prodi, E. Serra, and F. Marin, Phys. Rev. Lett. **112**, 023601 (2014).

[24] S. Sonar, V. Fedoseev, M. J. Weaver, F. Luna, E. Vlieg, H. van der Meer, D. Bouwmeester, and W. Löffler, Phys. Rev. A **98**, 013804 (2018).

[25] A. Borrielli *et al.*, Microsyst. Technol. **20**, 907 (2014).

[26] A. Borrielli *et al.*, Phys. Rev. B **94**, 121403(R) (2016).

[27] E. Serra *et al.*, AIP Adv. **6**, 065004 (2016).

[28] E. Serra, B. Morana, A. Borrielli, F. Marin, G. Pandraud, A. Pontin, G. A. Prodi, P. M. Sarro, and M. Bonaldi, J. Microelectromech. Syst. **27**, 1193 (2018).

[29] A. M. Jayich, J. C. Sankey, B. M. Zwickl, C. Yang, J. D. Thompson, S. M. Girvin, A. A. Clerk, F. Marquardt, and J. G. E. Harris, New J. Phys. **10**, 095008 (2008).

[30] A. Chowdhury *et al.*, Quantum Sci. Technol. **4**, 024007 (2019).

[31] A. Pontin, J. E. Lang, A. Chowdhury, P. Vezio, F. Marino, B. Morana, E. Serra, F. Marin, and T. S. Monteiro, Phys. Rev. Lett. **120**, 020503 (2018).

[32] See Supplemental Material at http://link.aps.org/supplemental/10.1103/PhysRevLett.124.023601 for the theoretical model.

[33] A. Szorkovszky, A. C. Doherty, G. I. Harris, and W. P. Bowen, Phys. Rev. Lett. **107**, 213603 (2011).

[34] A. Szorkovszky, G. A. Brawley, A. C. Doherty, and W. P. Bowen, Phys. Rev. Lett. **110**, 184301 (2013).

[35] M. Poot, K. Y. Fong, and H. X. Tang, Phys. Rev. A **90**, 063809 (2014).

[36] M. Poot, K. Y. Fong, and H. X. Tang, New J. Phys. **17**, 043056 (2015).

[37] A. Pontin, M. Bonaldi, A. Borrielli, L. Marconi, F. Marino, G. Pandraud, G. A. Prodi, P. M. Sarro, E. Serra, and F. Marin, Phys. Rev. Lett. **116**, 103601 (2016).